Supporting Information

Mechanism Investigations on Water Gas Shift Reaction over Cu(111), Cu(100) and Cu(211) Surfaces

Zhiyuan Li,[1]* Na Li,[1] Nan Wang,[1] Bing Zhou,[1] Pan Yin,[2] Boyu Song,[2] Jun Yu,[2] Yusen Yang[2]

[1] *Stated Grid Integrated Energy Service Group Co., Ltd., Beijing 100052, P. R. China*

[2] *State Key Laboratory of Chemical Resource Engineering, Beijing Advanced Innovation Center for Soft Matter Science and Engineering, Beijing University of Chemical Technology, Beijing 100029, P. R. China*

***** Corresponding author. Tel: +86-10-63505060; Fax: +86-10-63505555.

E-mail address: sailorlzy@163.com (Zhiyuan Li).

Contents

1. Adsorption site test

In order to find the most stable structures of all the species involved in the mechanism (H_2O, H_2, OH, O, H, CO, CO_2, COOH, CHO and HCOO) on Cu(111), Cu(100) and Cu(211) surfaces, several possible adsorption sites are tested.

The most stable adsorption structures of H_2O, OH, H, H_2, O, CO, CO_2, COOH, CHO and HCOO are top site, hollow site, hollow site, bridge site, hollow site, hollow site, top site, bridge site, bridge site and bridge site on the Cu(111) surface, respectively, as highlighted in red in **Figure S1**.

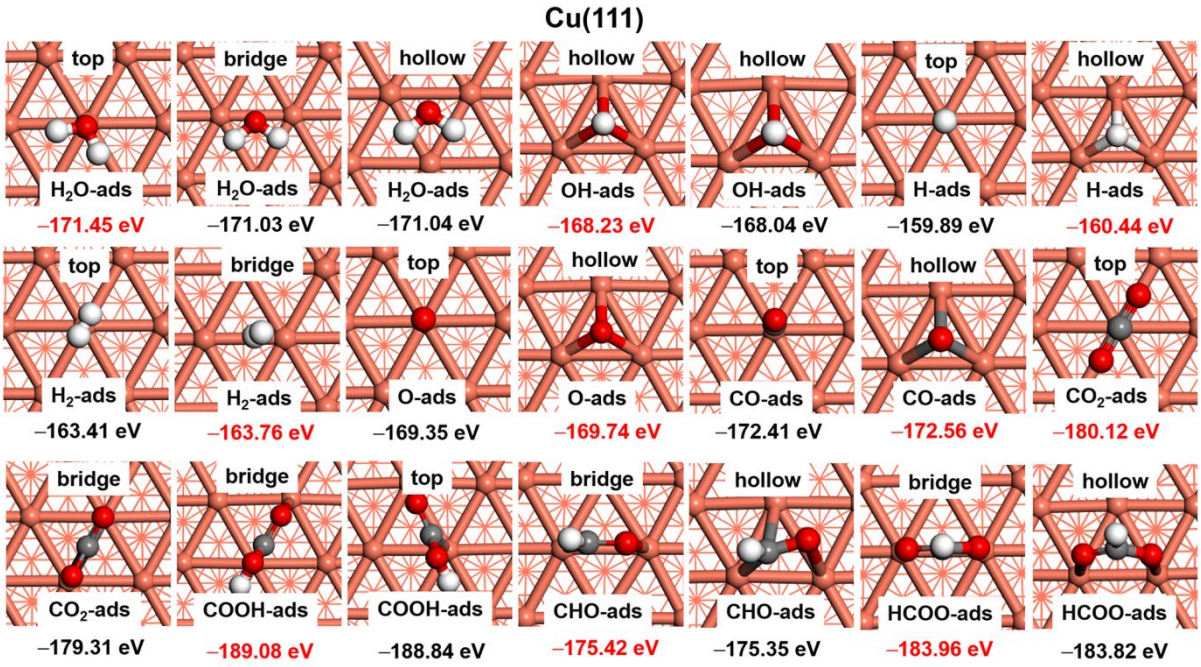

Figure S1. Summary of the possible adsorption structures of H_2O, OH, H, CO, CHO, CO_2, COOH, CHO and HCOO (including the top site, bridge site and hollow sites) on Cu(111) surface.

The most stable adsorption structures of H_2O, OH, H, H_2, O, CO, CO_2, COOH, CHO and HCOO are top site, hollow site, hollow site, top site, hollow site, hollow site, bridge site, hollow site and bridge site on the Cu(100) surface, respectively, as highlighted in red in **Figure S2**.

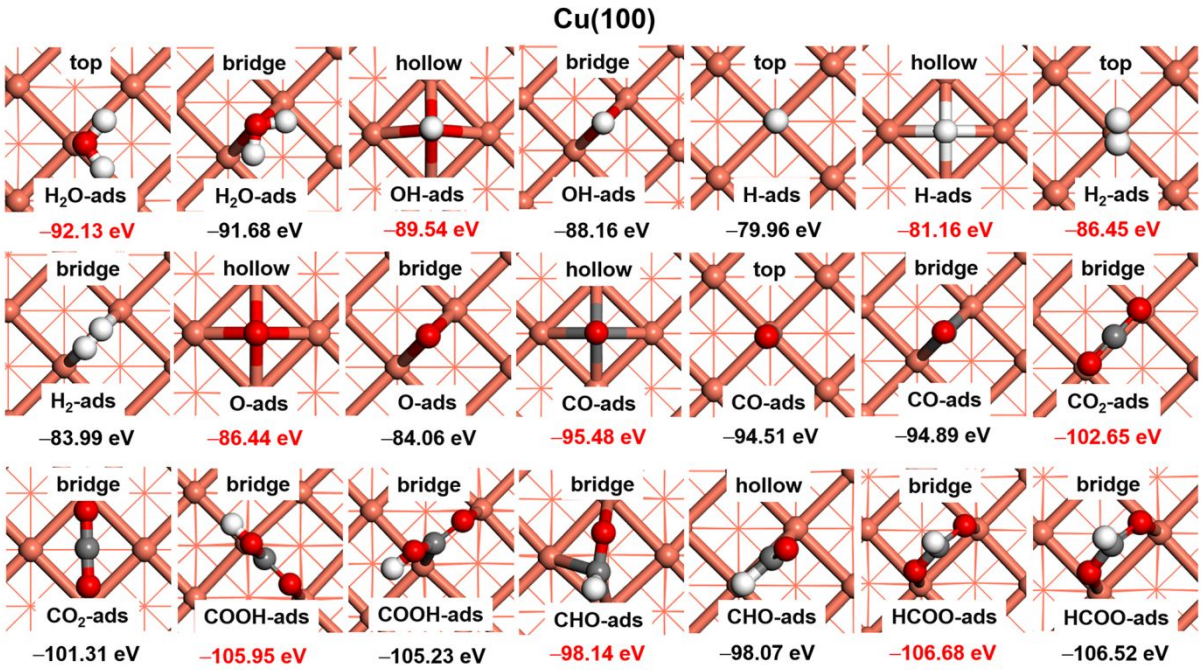

Figure S2. Summary of the possible adsorption structures of H_2O, OH, H, CO, CHO, CO_2, COOH, CHO and HCOO (including top site, bridge site and hollow site) on Cu(100) surface.

The most stable adsorption structures of H_2O, OH, H, H_2, O, CO, CO_2, COOH, CHO and HCOO are top site, bridge site, hollow site, hollow site, hollow site, hollow site, top site, bridge site, hollow site and bridge site on the Cu(211) surface, respectively, as highlighted in red in **Figure S3**.

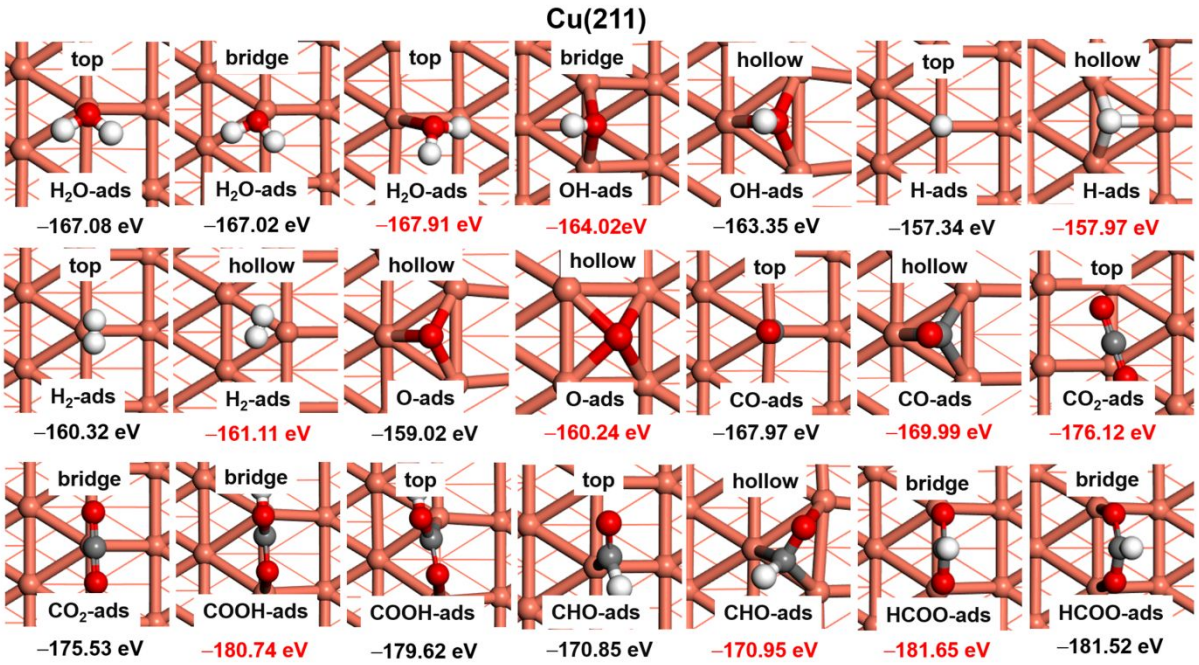

Figure S3. Summary of the possible adsorption structures of H_2O, OH, H, CO, CHO, CO_2, COOH, CHO and HCOO (including top site, bridge site and hollow site) on Cu(211) surface.

The binding energies values of Adsorbed species reported in the literatures are shown in the **Table S1**. Our calculation results have not significant difference from those reported in the literatures, which shows the reliability of our calculation results.

Table S1. Adsorption energies (E_{ads}, in eV) of species involved in the WGS reaction on Cu(111), Cu(100) and Cu(211) surfaces reported in the literatures

Species		**H_2O**	**CO**	**OH**	**H**	**H_2**	**CO_2**
Cu(111)	site	top	hollow	hollow	hollow	top	top
	E_{ads}	-0.18[S1]	-0.96[S2]	-2.85[S2]	-2.55[S2]	-0.02[S3]	-0.09[S2]
		PBE	PW91	PW91	PW91	PW91	PW91
Cu(100)	site	hollow	hollow	hollow	hollow	–	–
	E_{ads}	–0.25[S4]	–0.83[S4]	–3.51[S4]	–2.38[S4]		
		PW91	PW91	PW91	PW91		
Cu(211)	site	top	Hollow	bridge	hollow	–	–
	E_{ads}	–0.36[S5]	–0.91[S5]	–3.44[S5]	–2.48[S5]		
		PBE	PBE	PBE	PBE		

2. WGSR elementary reaction step on Cu(111), Cu(100) and Cu(211) surfaces

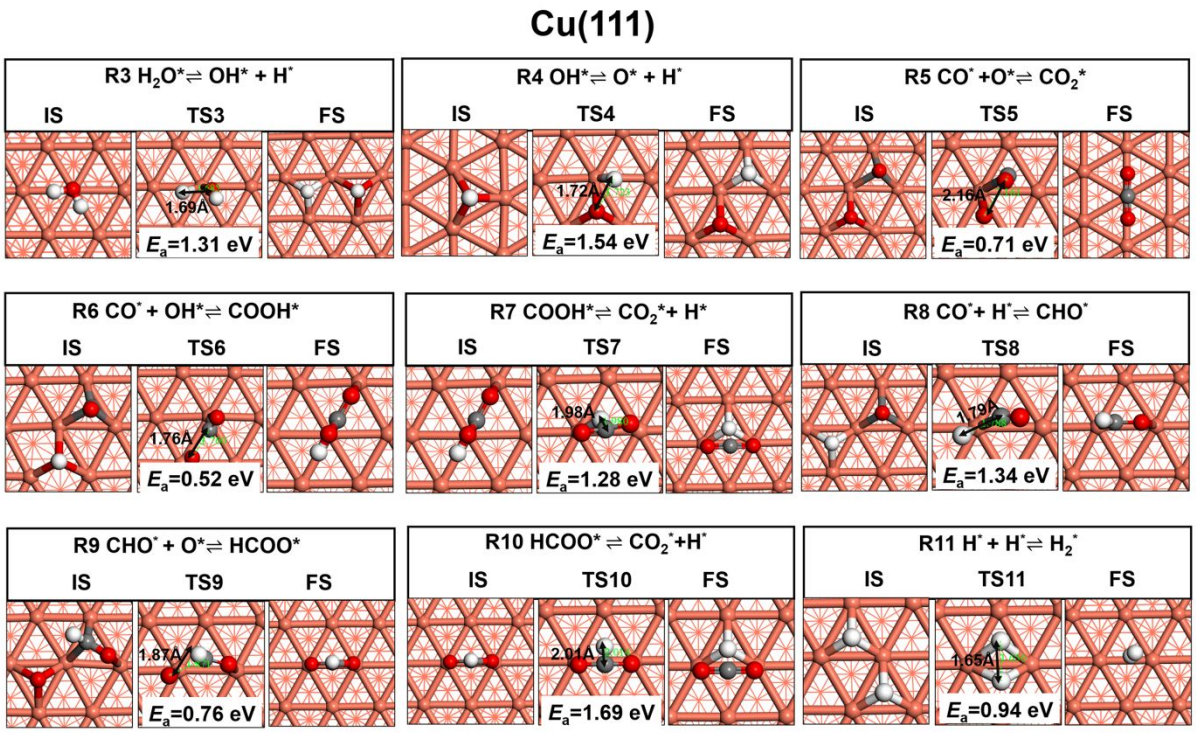

Figure S4. Initial state (IS), the corresponding transition state (TS) and final state (FS) structures and energies barrier(E_a) of WGSR element steps on the Cu(111) surface.

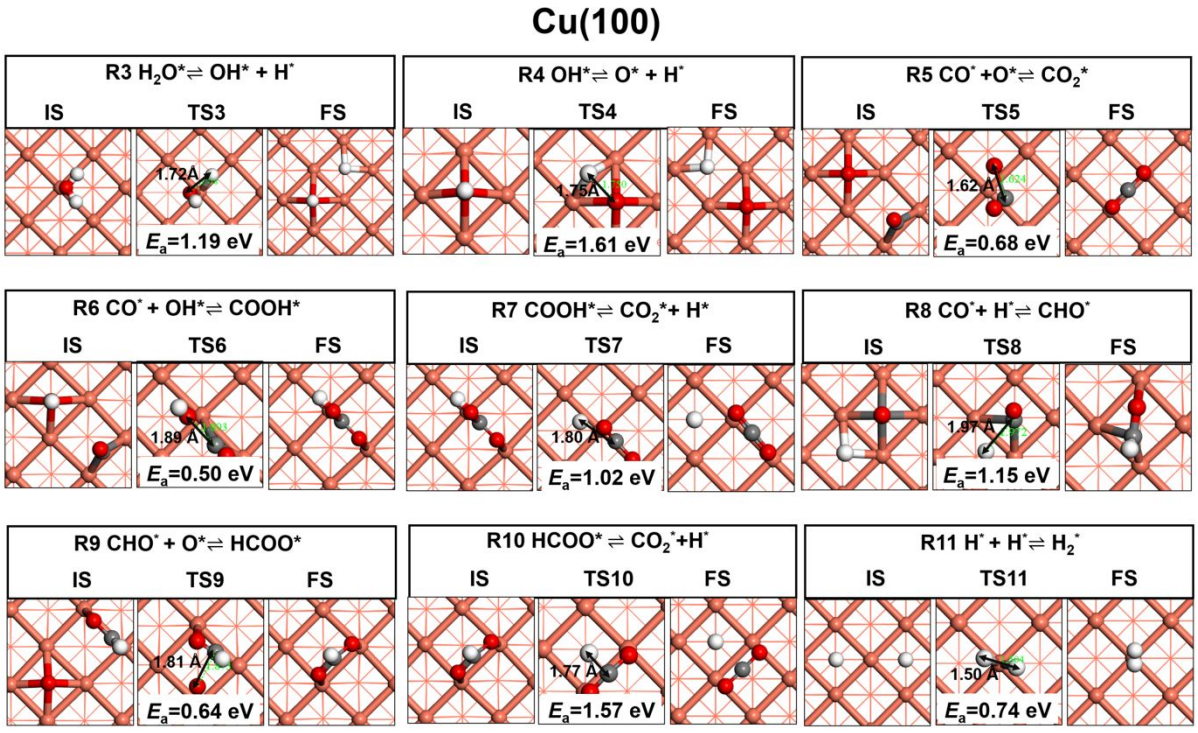

Figure S5. Initial state (IS), the corresponding transition state (TS) and final state (FS) structures and energies barrier(E_a) of WGSR element steps on the Cu(100) surface.

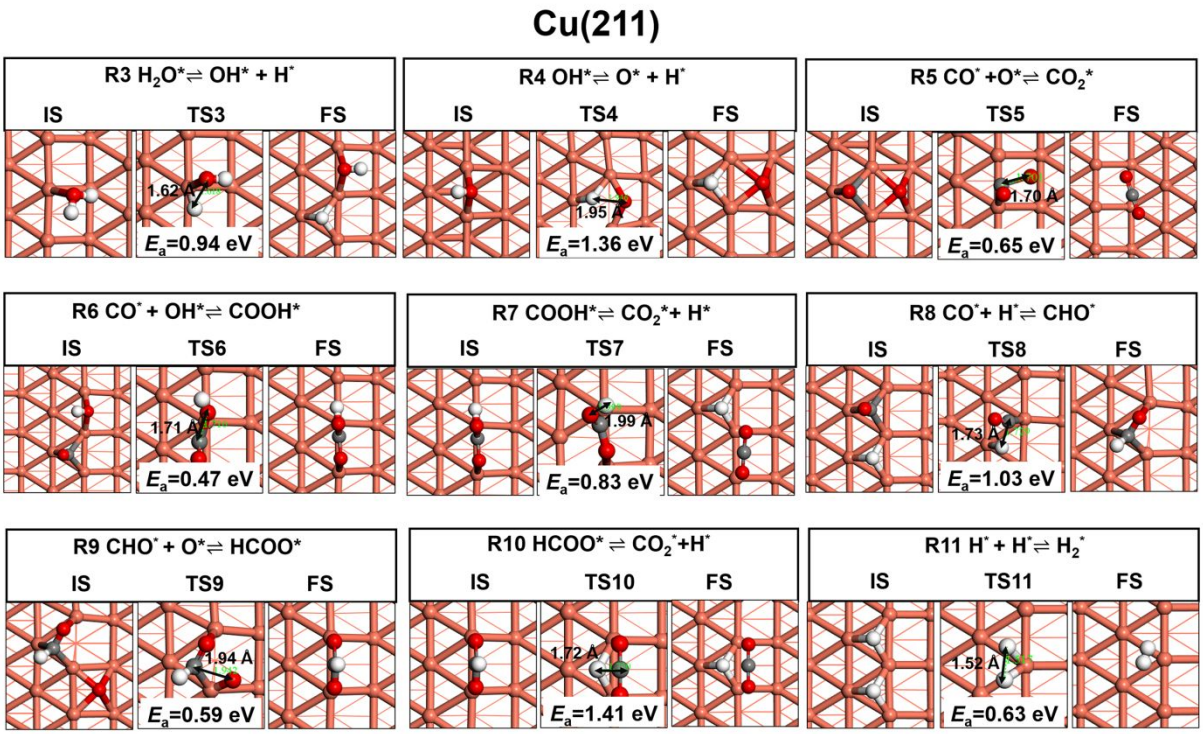

Figure S6. Initial state (IS), the corresponding transition state (TS) and final state (FS) structures and energies barrier (E_a) of WGSR element steps on the Cu(211) surface.

Table S2. The Total Energies (E), total Energies with entropy effect correction ($E_{entropy}$) of the reaction intermediates on the Cu(111), Cu(100) and Cu(211) surfaces

	Cu(111)		**Cu(100)**		**Cu(211)**	
R3	E/eV	$E_{entropy}$/eV	E/eV	$E_{entropy}$/eV	E/eV	$E_{entropy}$/eV
H_2O*	–177.43	–177.45	–94.13	–94.15	–168.91	–168.93
TS3	–176.12	–176.14	–92.94	–92.96	–167.97	–167.99
OH*+H*	–177.38	–177.39	–94.11	–94.13	–169.01	–169.03
R4	E/eV	$E_{entropy}$/eV	E/eV	$E_{entropy}$/eV	E/eV	$E_{entropy}$/eV
OH*	–173.86	–173.87	–90.54	–90.55	–165.45	–165.47
TS4	–172.32	–172.34	–88.93	–88.95	–164.08	–164.10
O*+H*	–173.25	–173.27	–89.97	–89.99	–164.38	–164.40
R5	E/eV	$E_{entropy}$/eV	E/eV	$E_{entropy}$/eV	E/eV	$E_{entropy}$/eV
CO*+ O*	–185.27	–185.28	–102.12	–102.14	–176.40	–176.42

TS5	–184.56	–184.57	–101.44	–101.46	–175.75	–175.77
CO_2*	–185.99	–186.01	–102.65	–102.66	–177.32	–177.34
R6	*E*/eV	$E_{entropy}$/eV	*E*/eV	$E_{entropy}$/eV	*E*/eV	$E_{entropy}$/eV
CO* + OH*	–189.46	–189.48	–106.26	–106.28	–181.00	–181.02
TS6	–188.94	–188.96	–105.76	–105.77	–180.53	–180.55
COOH*	–189.08	–189.10	–105.95	–105.96	–180.74	–180.76
R7	*E*/eV	$E_{entropy}$/eV	*E*/eV	$E_{entropy}$/eV	*E*/eV	$E_{entropy}$/eV
COOH*	–189.08	–189.10	–105.95	–105.97	–180.74	–180.76
TS7	–187.80	–187.82	–104.93	–104.95	–179.91	–179.93
CO_2* + H*	–189.65	–189.67	–106.33	–106.34	–180.95	–180.97
R8	*E*/eV	$E_{entropy}$/eV	*E*/eV	$E_{entropy}$/eV	*E*/eV	$E_{entropy}$/eV
CO* + H*	–176.41	–176.43	–98.94	–98.96	–173.59	–173.61
TS8	–175.07	–175.09	–97.79	–97.81	–172.57	–172.59
CHO*	–175.50	–175.52	–98.32	–98.34	–172.91	–172.93
R9	*E*/eV	$E_{entropy}$/eV	*E*/eV	$E_{entropy}$/eV	*E*/eV	$E_{entropy}$/eV
CHO* + O*	–188.02	–188.04	–105.00	–105.01	–179.65	–179.67
TS9	–187.26	–187.28	–104.36	–104.37	–179.06	–179.08
HCOO*	–189.97	–189.99	–106.69	–106.70	–181.65	–181.67
R10	*E*/eV	$E_{entropy}$/eV	*E*/eV	$E_{entropy}$/eV	*E*/eV	$E_{entropy}$/eV
HCOO*	–189.97	–189.98	–106.69	–106.704	–181.65	–181.67
TS10	–188.28	–188.29	–105.11	–105.13	–180.23	–180.25
CO_2 *+H*	–189.65	–189.67	–106.33	–105.35	–180.91	–180.93
R11	*E*/eV	$E_{entropy}$/eV	*E*/eV	$E_{entropy}$/eV	*E*/eV	$E_{entropy}$/eV
H*+ H*	–170.38	–170.39	–86.95	–86.97	–161.61	–161.62
TS11	–169.44	–169.46	–86.21	–86.23	–160.98	–160.99
H_2*	–169.80	–169.82	–86.45	–86.47	–161.11	–161.12

3. Determination of the effective barriers

The *TOF* can be simulated according to the energetic span theory[S6-S9] as follows:

$$E_a^{eff}\begin{cases} E_{TDTS}-E_{TDI} & \text{if TDTS appears after TDI} \quad \text{(a)} \\ E_{TDTS}-E_{TDI}+\Delta E & \text{if TDTS appears before TDI} \quad \text{(b)} \end{cases}$$

where k_B stands for the Boltzmann constant, T is the reaction temperature, and h is the Planck constant; E_a^{eff} is defined as an effective barrier of a catalysis process, based on the previous reports[S10,S11]: TDTS is the *TOF* determining transition state with the highest barrier; and TDI stands for the *TOF* determining intermediate, which is the most stable adsorption state along the energy profile, and ΔE is the reaction heat from reactant to TDI.

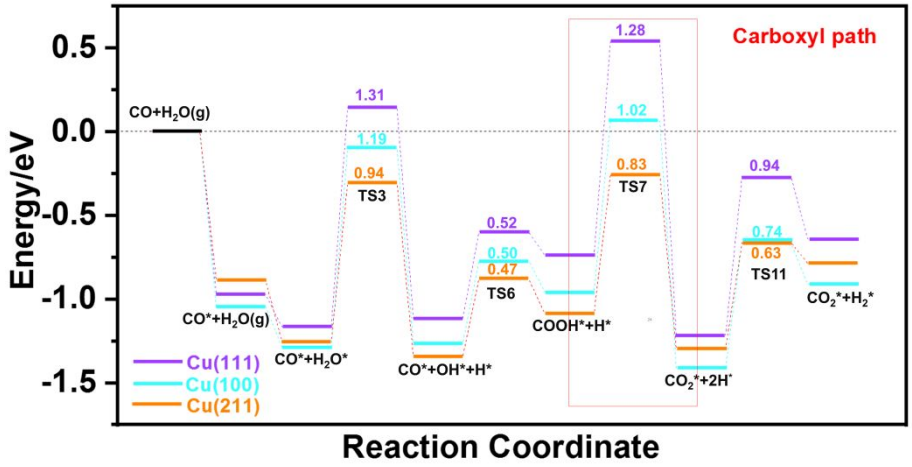

Figure S7. The energy profiles of carboxyl path of WGS reaction on the Cu(111), Cu(100) and Cu(211) surfaces. The numbers are the values of energy barriers (in eV) of the corresponding steps.

The essential aim here is to find a transition state (TS) – intermediate (I) pair with the largest energetic span (E_a^{eff}). The first step is to find the TDI, which should be first checked with the most stable adsorption state along the energy profile. The TDI are the adsorption state of CO_2*+2H* and the TDTS are the transition states of the COOH* dehydrogenation on Cu(111), Cu(100) and Cu(211) surfaces, respectively (**Figure S7**). As TDTS appears before TDI, we can calculate the E_a^{eff} with the eqn.(b). The value of E_a^{eff} is calculated to be 1.28 eV, 1.02 eV and 0.83 eV on Cu(111), Cu(100) and Cu(211) surfaces, respectively.

Table S3. The states of TDTS and TDI, the energies of TDTS and TDI, and the calculated E_a^{eff} of carboxyl path over Cu(111), Cu(100) and Cu(211) surfaces (see **Figure S7**)

	Cu(111)	Cu(100)	Cu(211)
TDTS	TS7	TS7	TS7
E_{TDTS}/eV	0.54	0.06	–0.26
TDI	CO_2*+2H*	CO_2*+2H*	CO_2*+2H*
E_{TDI}/eV	–1.22	–1.41	–1.29
ΔE/eV	–0.48	–0.45	–0.21
E_a^{eff}	1.28	1.02	0.83

4. Structural details of Cu

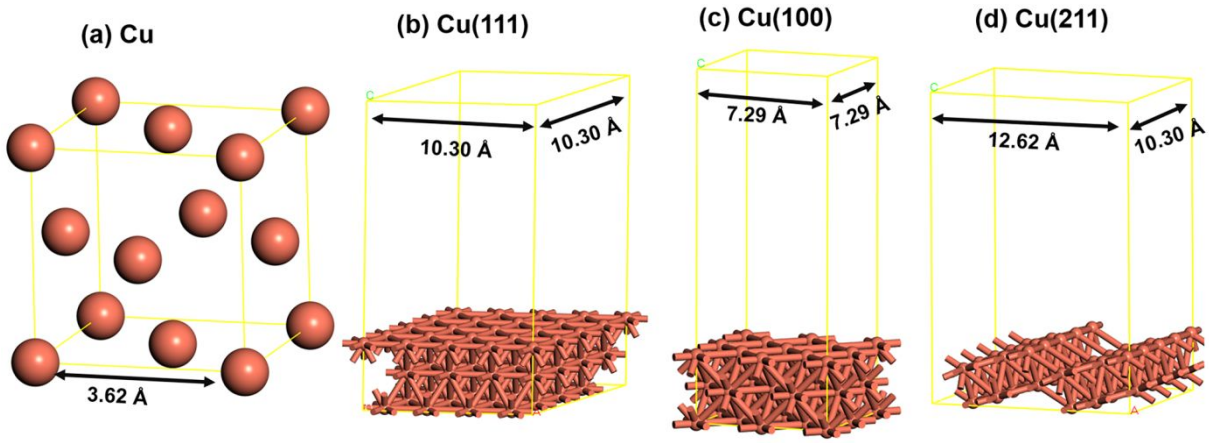

Figure S8. Structure details of (a) bulk Cu with its corresponding surfaces cleaved from bulk truncation (b) Cu(111), (c) Cu(100), and (d) Cu(211) (Cu: brown).

5. Supercell convergence test of Cu(111), Cu(100) and Cu(211) surfaces

The periodic calculation may influence the binding energy due to the lateral interaction.[S12] In order to test the supercell size of the calculation models, the models of Cu(111), Cu(100) and Cu(211): supercell 2×2; supercell 3×3; supercell 4×4; with H_2O absorbed, are optimized. The optimized structures are shown in **Figure S9**. The adsorption energies of H_2O on different supercells

are almost the same. Thus, the model with 2×2 supercell is employed in this work is relatively reasonable.

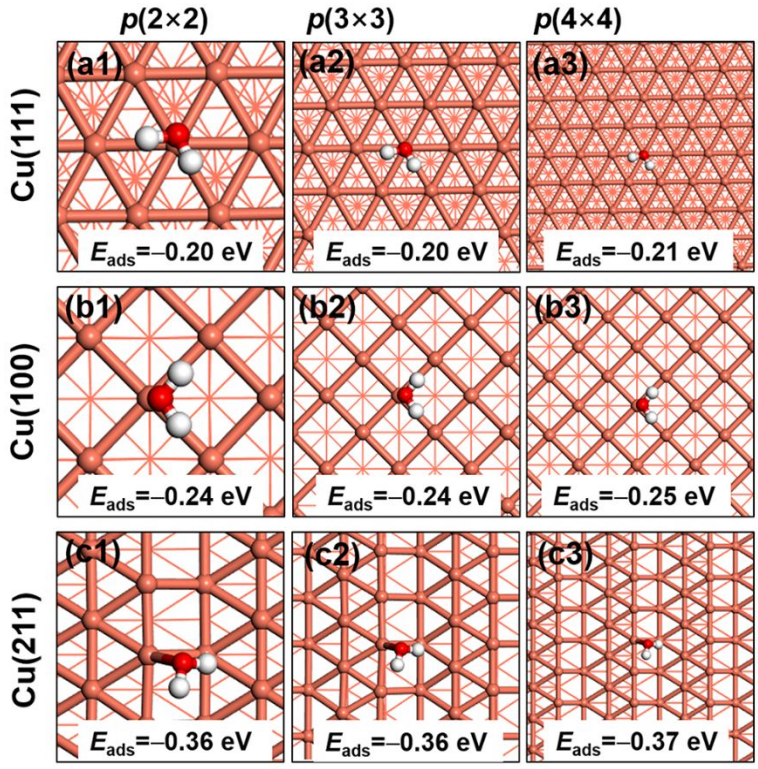

Figure S9. The adsorption energies (E_{ads}) of H_2O on 2×2, 3×3, 4×4 supercell of Cu(111), Cu(100) and Cu(211) surfaces, respectively.

6. Computational methods test

It can be found from the data in **Table S4** that the unit cell parameters of Cu (3.643 Å) obtained by the PBE method in our work are the closest to the experimental values (3.615 Å), the relative error is 0.77%, which is smaller than those calculated by the RPBE and PBEsol methods, respectively. In addition, the adsorption energies of H_2O on Cu(111) are compared (**Table S5**), and it is found that these values are relatively close. Therefore, it is very reasonable to use the PBE method for simulation calculations.

Table S4. Lattice parameters (in Å) of bulk Ni as calculated with different functions and comparison to experiment

Method	Lattice constant	Relative error
PBE	$a=b=c=3.643$	0.77%
RPBE	$a=b=c=3.680$	1.80%
PBEsol	$a=b=c=3.573$	–1.80%
Expt.	$a=b=c=3.615$[S13]	–

Table S5. The adsorption energy of H_2O on Cu(111) surface as calculated with different functions

Method	$E_{ads}(H_2O)$
PBE	–0.20
RPBE	–0.14
PBEsol	–0.36

The van der Waals (vdW) interactions are described using the long range dispersion correction (DFT-D) approach. As exhibited in **Figure S10** and **Table S6**, the adsorption energies of H_2O on Cu(111),Cu (100) and Cu(211) surfaces are enhanced when considering dispersion correction, and it can be seen that the dispersion force only affects the energy, but not the geometry.[S14] And the change trend of adsorption energy is consistent with the uncorrected data. Thus the structure data results in our work are relatively reasonable.

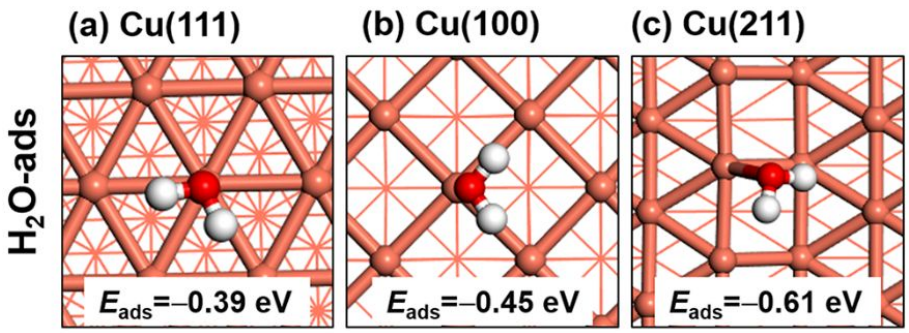

Figure S10. Adsorption structures and energies with dispersion correction of H_2O on (a) Cu(111), (b)

Cu(100) and (c) Cu(211) surfaces.

Table S6. Adsorption energies (E_{ads}), adsorption energies with dispersion correction (E_{disp}) of H_2O

H_2O-ads	E_{ads} (eV)	E_{disp} (eV)
Cu(111)	–0.20	–0.39
Cu(100)	–0.24	–0.45
Cu(211)	–0.36	–0.61

The fitting plots of the d-band center vs adsorption energies of H_2*, CO_2*, OH*, H*, O* on Cu(111), Cu(100) and Cu(211) surfaces are shown in **Figure S11**. CO_2, H_2 and H adsorb very weakly on Cu(111), Cu(100) and Cu(211) through van der Waals interaction. With the change of the center of the d-band, the adsorption energy does not change significantly. While the increase in d-band center resulted in increase in adsorption strength of OH* and O*, which is in consistent with the d-band center theory.

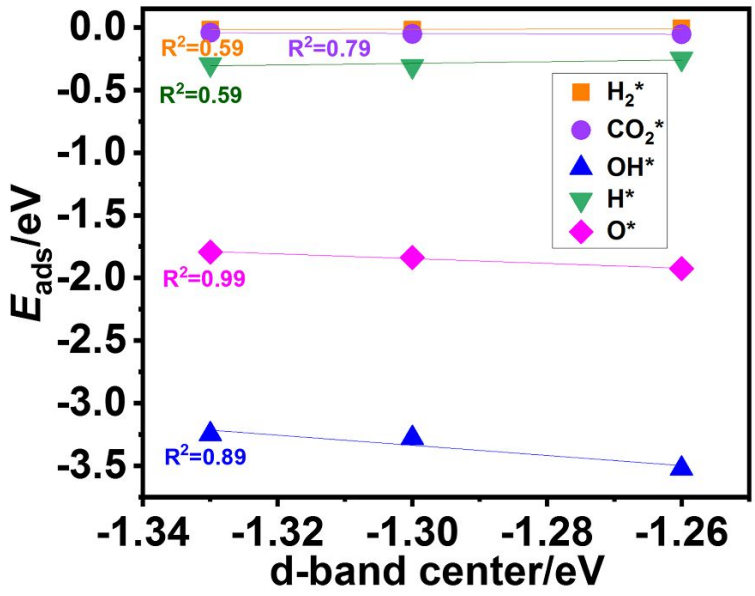

Figure S11. The fitting plot of d-band center *vs*. adsorption energies (E_{ads}) of H_2*, CO_2*, OH*, H* and O* on Cu(111), Cu(100) and Cu(211) surfaces.

References

(S1) Fajín, J. C.; Illas, F.; Gomes, J. R. B. Effect of the Exchange-Correlation Potential and of Surface Relaxation on the Description of the H_2O Dissociation on Cu(111). *J. Chem. Phys.* **2009**, *130*, 224702-224710.

(S2) Gokhale, A. A.; Dumesic, J. A.; Mavrikakis, M. On the Mechanism of Low-Temperature Water Gas Shift Reaction on Copper. *J. Am. Chem. Soc.* **2008**, *130*, 1402-1414.

(S3) Tang, Q.; Chen, Z. X.; He, X. A Theoretical Study of the Water Gas Shift Reaction Mechanism on Cu(111) Model System. *Surf. Sci.* **2009**, *603*, 2138-2144.

(S4) Wang, G.; Nakamura, J. J. Structure Sensitivity for Forward and Reverse Water-Gas Shift Reactions on Copper Surfaces: A DFT Study. *J. Phys. Chem. Lett.* **2010**, *1*, 3053-3057.

(S5) Roy, S.; Tiwari, A. K. Efficient Water-Gas Shift Catalysts for H_2O and CO Dissociation Using Cu-Ni Step Alloy Surfaces. *J. Phys. Chem. C* **2021**, *125*, 13819-13835.

(S6) Kozuch, S.; Shaik, S. A Combined Kinetic-Quantum Mechanical Model for Assessment of Catalytic Cycles: Application to Cross-Coupling and Heck Reactions. *J. Am. Chem. Soc.* **2006**, *128*, 3355-3365.

(S7) Kozuch, S.; Shaik, S. How to Conceptualize Catalytic Cycles? The Energetic Span Model. *Acc. Chem. Res.* **2010**, *44*, 101-110.

(S8) Kozuch, S.; Martin, J. M. L. What Makes for a Bad Catalytic Cycle? A Theoretical Study on the Suzuki-Miyaura Reaction within the Energetic Span Model. *ACS Catal.* **2011**, *1*, 246-253.

(S9) Kozuch, S.; Martin, J. M. What Makes for a Good Catalytic Cycle? A Theoretical Study of the Sphos Ligand in the Suzuki-Miyaura Reaction. *Chem. Commun.* **2011**, *47*, 4935-4937.

(S10) Yang, B.; Burch, R.; Hardacre, C.; Hu, P.; Hughes, P. Selective Hydrogenation of Acetylene over Pd-Boron Catalysts: A Density Functional Theory Study. *J Phys. Chem. C* **2014**, *118*, 3664-3671.

(S11) Yang, B.; Burch, R.; Hardacre, C.; Headdock, G.; Hu, P. Influence of Surface Structures, Subsurface Carbon and Hydrogen, and Surface Alloying on the Activity and Selectivity of Acetylene Hydrogenation on Pd Surfaces: A Density Functional Theory Study. *J. Catal.* **2013**, *305*, 264-276.

(S12) Carvalho, T. P.; Catapan, R. C.; Oliveira, A. A. M.; Vlachos, D. G. Microkinetic Modeling and Reduced Rate Expression of the Water-Gas Shift Reaction on Nickel. *Ind. Eng. Chem. Res.* **2018**, *57*, 10269-10280.

(S13) Otte, H. M. Lattice Parameter Determinations with an X-Ray Spectrogoniometer by the Debye-Scherrer Method and the Effect of Specimen Condition. *J. Appl. Phys.* **1961**, *32*, 1536.

(S14) Zhou, Y.; Sun, W.; Chu, W.; Zheng, J.; Gao, X.; Zhou, X.; Xue, Y. Adsorption of Acetylene

on Ordered Ni_xAg_{1-x}/Ni (111) and Effect of Ag-Dopant: A DFT Study. *Appl. Surf. Sci.* **2018**, *435*, 521-528.